Noncontrast-Enhanced Three-Dimensional (3D) Intracranial MR Angiography Using Pseudocontinuous Arterial Spin Labeling and Accelerated 3D Radial Acquisition

Huimin Wu,[1]* Walter F. Block,[1–3] Patrick A. Turski,[2] Charles A. Mistretta,[1,2] and Kevin M. Johnson[1]

Pseudocontinuous arterial spin labeling (PCASL) can be used to generate noncontrast magnetic resonance angiograms of the cerebrovascular structures. Previously described PCASL-based angiography techniques were limited to two-dimensional projection images or relatively low-resolution three-dimensional (3D) imaging due to long acquisition time. This work proposes a new PCASL-based 3D magnetic resonance angiography method that uses an accelerated 3D radial acquisition technique (VIPR, spoiled gradient echo) as the readout. Benefiting from the sparsity provided by PCASL and noise-like artifacts of VIPR, this new method is able to obtain submillimeter 3D isotropic resolution and whole head coverage with a 8-min scan. Intracranial angiography feasibility studies in healthy (N = 5) and diseased (N = 5) subjects show reduced saturation artifacts in PCASL-VIPR compared with a standard time-of-flight protocol. These initial results show great promise for PCASL-VIPR for static, dynamic, and vessel selective 3D intracranial angiography. **Magn Reson Med 69:708–715, 2013.**

Key words: magnetic resonance angiography; pseudocontinuous arterial spin labeling; cerebrovascular disease; VIPR = vastly undersampled isotropic projection reconstruction; three-dimensional imaging

INTRODUCTION

Cerebrovascular disease is the third leading cause of mortality in the United States accounting for approximately 200,000 deaths in the US each year as well as considerable neurologic morbidity (1). Imaging of the cerebral vasculature system is paramount for both diagnosis and treatment planning. X-ray digital subtraction angiography (DSA) has long been considered the reference standard for cerebral angiography with modern protocols now allowing for extremely high resolution, three-dimensional (3D) static imaging as well as vessel selective, dynamic two-dimensional (2D) projection imaging. However, X-ray DSA poses risk to patients due to the need for invasive access, ionizing radiation, and iodinated contrast agents. Additionally, X-ray DSA provides an incomplete assessment of tissue damage. Magnetic resonance imaging is capable of assessing disease markers including tissue viability (2), perfusion (3), and hemorrhage (4). Unfortunately, magnetic resonance angiography (MRA) is severely lacking compared with X-ray DSA. Intracranial MRA is most frequently performed with 3D time-of-flight (TOF) with multiple overlapping thin slabs (5). This technique provides relatively high spatial resolution; however, it is limited by the saturation of spins in slow, complex, or in-plane flow (6) and provides limited information of vessel filling patterns.

Developing techniques hold the potential to significantly improve intracranial MRA. Contrast-enhanced MRA, which has proven to be robust in the extracranial vasculature, is highly challenging in the cerebral vasculature due to the rapid passage of blood from arteries to veins. However, contrast-enhanced MRA has reaped the benefits of accelerated imaging strategies (7–9) and is now feasible for intracranial imaging, albeit at relatively low spatial resolutions compared with X-ray DSA. Noncontrast-enhanced technique has seen renewed development since the discovery of nephrogenic systemic fibrosis (10,11). One of these techniques, arterial spin labeling (ASL), is of particular interest for intracranial applications. Similar to TOF, ASL relies on the inflow of blood into the imaging volume; however, ASL uses separate sequences to label and image inflowing spins. By subtracting the images with different labeling sequences, angiography can be obtained with near zero background, vessel selectivity, and inflow dynamics similar to X-ray DSA. Although ASL has been in development since 1987 (12), its use in angiography has been limited due to low signal-to-noise ratio (SNR), long scan times, and difficulties in practical implementation.

ASL magnetic resonance imaging can be divided into two basic types: pulsed ASL (PASL) and continuous ASL (CASL). PASL uses a single inversion pulse and has been popular in the last decades due to its easy implementation. With recent improvements in accelerated imaging, promising intracranial results have been shown using PASL with spoiled gradient echo (SPGR) for static angiography (13). Unfortunately, PASL angiography is highly sensitive to the selection of inversion time, is

[1]Department of Medical Physics, University of Wisconsin, Madison, Wisconsin, USA.
[2]Department of Radiology, University of Wisconsin, Madison, Wisconsin, USA.
[3]Department of Biomedical Engineering, University of Wisconsin, Madison, Wisconsin, USA.

Grant sponsor: NIH; Grant number: R01NS066982.

*Correspondence to: Huimin Wu, M.S., Department of Medical Physics, Wisconsin Institutes Medical Research, 1111 Highland Avenue, Room 1005, Madison, WI 53705-2275. E-mail: hwu7@wisc.edu

Received 23 January 2012; revised 16 March 2012; accepted 27 March 2012.
DOI 10.1002/mrm.24298
Published online 24 April 2012 in Wiley Online Library (wileyonlinelibrary.com).

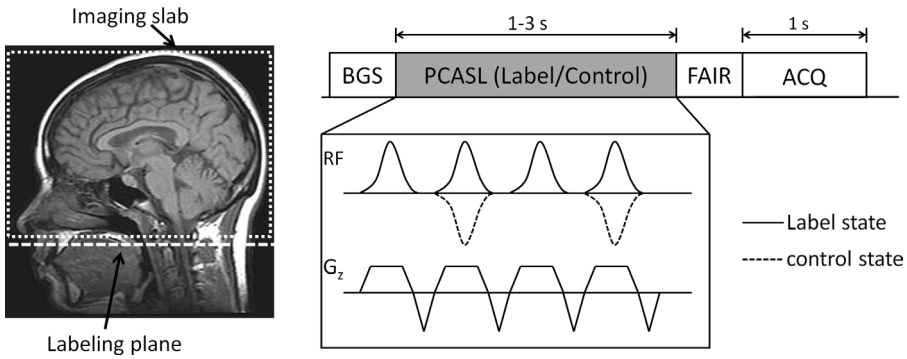

FIG. 1. Labeling geometry (left, white dashed box indicates imaging slab, dashed line indicates the labeling plane); PCASL-VIPR sequence diagram (right) shows a tag session consisting of four modules: background suppression, PCASL, flow-alternating inversion recovery, and image acquisition with time assignment. PCASL is set to label state or control state to acquire the label image and the control image, respectively.

subjected to blurring due to tag decay during the readout, and the extent of the labeling is limited by the field homogeneity of the excitation radio frequency. Inversion time resolved, balanced steady-state free precession (bSSFP) not only offers the potential to retrospectively choose inversion time with reduced blurring (14–17) but also introduces substantial artifacts from the bSSFP readout.

CASL techniques use flow-driven adiabatic inversion to produce higher SNR images with reduced sensitivity to inversion time. However, these techniques have been challenging in practical implementation, and therefore have not been used widely. Recently, a new strategy for CASL has been reported referred to as pseudocontinuous ASL (PCASL) (18,19), which allows practical implementation without specialized hardware. In an initial extracranial comparison, PCASL has been demonstrated to provide significantly higher arterial signal compared with PASL and improve diagnostic confidence (20). PCASL also holds the potential to provide hemodynamic information and label the selected vessels similar to X-ray DSA (21,22). Unfortunately, current intracranial angiography is limited to 2D projection imaging or low-resolution 3D imaging due to scan time limitations. For example, recent 2D projection imaging has required 11 s per slice (21), which translates to scan times over 30 min for true 3D imaging even with parallel imaging.

In this work, we propose an accelerated PCASL-based 3D MRA technique that uses a 3D radial acquisition technique called vastly undersampled isotropic projection reconstruction (VIPR) (23). Benefiting from the highly sparse image volume created by PCASL, and noise-like artifacts specific to 3D radial acquisition, PCASL-VIPR can achieve whole head coverage and submillimeter isotropic spatial resolution within clinically acceptable scan time. Feasibility studies have been conducted in both normal subjects and patients with both qualitative and quantitative comparison against 3D TOF.

METHODS

Sequence

PCASL angiography is performed with an interleaved acquisition set to two tagging states, control and label, which are subtracted to yield an angiographic image. Each tag session consists of four modules: background saturation, PCASL, PASL, and imaging, as illustrated in Fig. 1.

For background suppression, we used a variable rate selective excitation (VERSE) transformed hyperbolic secant pulse (24) to selectively invert the imaging slab. This helps to reduce the signal from cerebrospinal fluid and other background tissue that give rise to artifacts.

The PCASL module was implemented following a balanced gradient approach (19) using a train of pulsed radiofrequency (RF) and gradients as illustrated in Fig. 1. In the label state, the RF phase cycling is set such that spins at the labeling plane see RF pulses with the same phase. In this condition, the spins passing through this labeling plane undergo adiabatic inversion. In the control state, the RF pulse train and the gradients are the same as in the label state, while the RF phase is cycled such that spins at the labeling plane see RF pulses having a phase of π relative to the previous pulse, leading to limited effect on the passing spins. In our implementation, a Hanning window-shaped RF pulse of 500 μs duration was performed periodically with a 1200 μs spacing between RF pulses. The amplitude of the RF pulse and gradients were optimized using Bloch simulation to get a labeling efficiency greater than 95%. The parameters we used in this study are as follows: average gradient = 0.78 mT/m, maximum gradient = 7 mT/m, average $B_1 = 1.63$ μT.

At the end of PCASL labeling, inflowing spins superior to the labeling plane are inverted. However, fresh spins will displace labeled spins during the imaging module causing signal loss in proximal vessels. This could be avoided by setting a large gap between the labeling plane and the inferior edge of the image region. However, this will lead to substantial reduction in SNR and adds a transit time parameter that will vary from subject to subject depending on the flow velocity. To avoid signal loss with SNR penalty, we followed the scheme in Ref. 21 to incorporate a PASL scheme at the end of PCASL to ensure a continued inflow of labeled blood during image acquisition. In our study, flow-alternating inversion recovery (25) is implemented such that a selective inversion pulse is applied on the imaging slab in label state, while a global inversion pulse in

control state. By doing this, the label image contains uninverted blood spins, whereas the control image contains inverted blood spins. The tissue spins are inverted in both images and canceled out in the final subtracted image.

Both bSSFP and SPGR have been used for noncontrast angiography and can be used as readout with PCASL. bSSFP provides substantially higher signal; however, bSSFP is highly sensitive to off resonance, leads to high specific absorption rate, and can be sensitive to flow related artifacts (26). Off-resonance artifact is a particular issue in intracranial applications, due to susceptibility at the skull base and nasal fossa, movement of spins through the off-resonant field, and higher utilization of 3T scanners. To avoid these artifacts, the acquisition module consists of a low flip angle SPGR readout combined with a VIPR sampling strategy.

The VIPR sequence samples data along radial lines evenly spaced through a spherical volume each intersecting the origin of k-space. For PCASL angiography, VIPR has two major advantages over Cartesian acquisitions. First, undersampling artifacts appear as a diffuse low-level background noise rather than ghosting artifacts in Cartesian acquisitions (27). This allows for undersampling acceleration when the image is sparse. The subtractive nature of PCASL creates a highly sparse imaging volume allowing the high acceleration factors needed to keep the scan time in a clinical acceptable range for 3D scans. Second, 3D radial sampling is more robust to contrast changes during the acquisition. During the readout, the signal experience T_1 recovery and RF saturation due to repetitive RF pulses. This signal behavior approximately follows the exponential decay curve for spins in the volume. Previous work with Cartesian angiography (13) and fast spin echo imaging have well characterized the response to the decay as an apodization in k-space, which results in the loss of spatial resolution. For 3D radial acquisition, the signal modulation leads to an increased angular undersampling artifact in the image as demonstrated in previous applications of radial acquisition for hyperpolarized He3 magnetic resonance imaging (28) and fast spin echo (29,30). This is merely due to the fact that the decay is evenly distributed between the edge and center of the k-space. The additional diffuse artifacts have no effects on the image resolution, which makes VIPR advantageous for angiography where high resolution is critical.

Evaluation

Five healthy volunteers (one women, four men, age range 25–35) and five patients with previously diagnosed arteriovenous malformations (AVMs) ($N = 3$) or aneurysms ($N = 2$) were imaged after obtaining Institutional Review Board approval and informed consent. All exams were performed on a clinical 3T magnetic resonance system (Discovery 750; GE Healthcare, Waukesha, WI) with a 32-channel head coil (Nova Medical, Wilmington, MA) for reception and body coil for transmission. Subjects were imaged with a clinical standard 3D TOF scan and a whole brain PCASL-VIPR scan. The standard 3D TOF scan was acquired with the following parameters: TR/TE 30/2.8; field of view 22 $\times$ 22 cm^2; matrix 512 $\times$ 256; slice thickness 1 mm; flip angle 20°; bandwidth $\pm$41.67 kHz; number of slabs 4 (an exception is the case with a basilar tip aneurysm where only two oblique slabs were acquired and the scan time is 4 min); slab thickness 40 mm; overlap thickness 10 mm; parallel imaging method SENSE (ASSET; GE Healthcare) with an acceleration factor of 2$\times$. For partial head coverage of 11 cm, the examination time was 8:01 min.

For PCASL-VIPR scan, the labeling plane is approximately placed at C1 segment of the internal carotid arteries such that the major feeding arteries of the brain vasculature including internal carotid arteries, external carotid arteries, and vertebral arteries will be labeled. A 16-cm-thick imaging slab was prescribed right above the labeling plane covering the whole brain. PCASL-VIPR parameters include: labeling duration 3 s; image acquisition window 1 s; field of view 22 $\times$ 22 $\times$ 16 cm^3; 3D isotropic resolution 0.68 mm; readout bandwidth $\pm$62.50 kHz; TR/TE(ms) 5.06/1.07; fractional echo 0.75; flip angle 10°; no flow compensation. A total of 12,000 projections were collected in a scan time of 8:27 min. Compared to Nyquist, this represents a 13$\times$ undersampling. Data acquired for the label image and control image are first subtracted in k-space then reconstructed using an optimized gridding routine (31) zero-filled to 0.46 mm isotropic resolution. Individual coil images were combined using coil sensitivities estimated from the center of k-space (32). This coil combination helps reduce undersampling artifacts as in partially parallel imaging with localized sensitivity (PILS) (33) and leads to more optimal SNR in the final image (34).

Images from 3D TOF and PCASL-VIPR were evaluated quantitatively and qualitatively. For qualitative evaluation of image quality, two experienced readers (one senior neuroradiologist and one senior investigator with over 25 years of experience in neurovascular imaging research) were presented with source images from both 3D TOF and PCASL-VIPR scans on a radiology workstation (Horizon Rad Station, version 11.8, McKesson, San Francisco, CA). The grading was not blinded as the PCASL and 3D TOF exams could be readily distinguished by the presence or absence of slab artifact and residual background signal on the 3D TOF studies. PCASL-VIPR and 3D TOF examinations were evaluated using two criteria (vessel visualization and saturation artifacts), defined on a four-point scale (Table 1). Eight vessel segments were evaluated for each subjects, whereas pathology was evaluated only for the patients. Pearson correlation test was performed to assess the inter-rater correlation of the grading of the two readers. The nonparametric Wilcoxon signed rank method was used to test for a significant difference in image quality between PCASL-VIPR and 3D TOF for each criterion, where $P < 0.05$ was taken to be statistically significant.

For quantitative evaluation, regions of interest (ROIs) were placed on the source images of the five healthy subjects on the following locations: siphons (left/right), basilar tip, carotid terminus (left/right), first bifurcation of middle cerebral artery (left/right), 5-mm region around the anterior communicating artery, and background tissue. Contrast-to-noise ratio (CNR) was measured with equation

Table 1
Criteria for Qualitative Evaluation

Criterion	Interpretation	Score
Vessel visualization	Nondiagnostic or not visible	1
	Poor (structures visible but with significant blurring or artifacts, nondiagnostic)	2
	Good (good quality diagnostic information, minimal blurring, or artifacts)	3
	Excellent (excellent quality diagnostic information, sharply defined borders)	4
Saturation artifacts	Severe signal dropouts. Not diagnostic	1
	Moderate signal dropouts. Loss of diagnostic accuracy	2
	Minimal presence of signal dropouts. Does not interfere with diagnostic interpretation	3
	No significant saturation artifacts	4

CNR = $(V - B)/\sigma$, where V represents the maximum signal in ROIs, B represents the average signal in background ROIs, and σ is the standard deviation of the signals in background ROIs. For PCASL-VIPR images, σ includes the noise and also undersampling artifacts that have noise-like appearance. The Student's t test was performed to test for a significant difference in mean CNR between PCASL-VIPR and 3D TOF for each vessel groups.

RESULTS

Figure 2 shows representative PCASL-VIPR images obtained in a healthy subject. With near-zero background, whole volume maximum intensity projections (MIPs) could be generated at any angle. The axial, coronal, and sagittal collapsed views are presented. High spatial resolution enables visualization of small distal arteries with size of submillimeter. Signal intensity decays from proximal to distal vessels due to T_1 recovery and RF saturation. Whole brain coverage is achieved with a 16-cm slab thickness.

Figure 3 shows results of a patient with a thalamic AVM with deep venous drainage. Limited MIPs in the sagittal view of the same thickness and location were performed for the source images of both PCASL-VIPR and 3D TOF. Images were cropped to compare with X-ray DSA image, which was also performed for this patient as the reference standard. The images show increased flow through the left posterior cerebral artery and the venous drainage into the vein of Galen. The structures of the AVM were equally visualized in both exams with delineation of the main feeding arteries confirmed by X-ray DSA. However, severe signal loss in the draining vein due to saturation can be observed in the TOF image.

Figure 4 shows results of a patient with left frontal AVM. From the limited sagittal MIP images of both exams, it is easy to distinguish the left anterior cerebral artery as the dominant supply to the AVM. High signal in the feeders in the PCASL-VIPR MIP image suggests short transit time from the labeling plane due to fast flow. There is still mild signal loss due to saturation in the feeding arteries in the TOF image. The superficial venous drainage can be observed in both exams.

Figure 5 shows results of a patient with a small aneurysm located at the tip of the basilar artery. The limited sagittal MIP images and the zoomed in view at the location of the disease of both exams show excellent depiction of the aneurysm. Because of the fast flow in the aneurysm and small size, little saturation artifact was seen in TOF image that would affect the visualization of the aneurysm. The inflow jet of the aneurysm that is shown as a bright region (arrows) is depicted in both images.

Figure 6 shows results of a patient with a large aneurysm arising from the left cavernous internal carotid artery. Limited coronal MIPs of both exams are shown at the aneurysm location. A profile was drawn along a horizontal line (indicated with a white line) through the aneurysm for the two MIP images. Signal intensity was scaled for the two profiles to be compared together. The profile of TOF shows signal drop both in the region of the aneurysm and the left carotid artery compared to the left side. This is likely caused by the saturation artifacts due to the slow, recirculating flow inside the aneurysm.

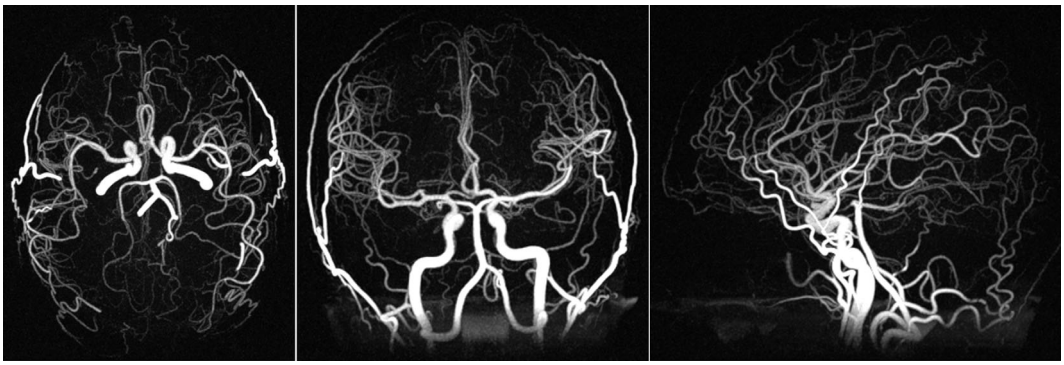

FIG. 2. Axial, coronal, and sagittal MIPs of PCASL-VIPR of a healthy subject (for better visualization, a few slices at the inferior edge of the 3D image volume were excluded when performing axial MIP). Images show complete filling of the entire arterial vasculature of the brain. Signal intensity decreases from proximal to distal vessels due to increasing transit time from the labeling plane.

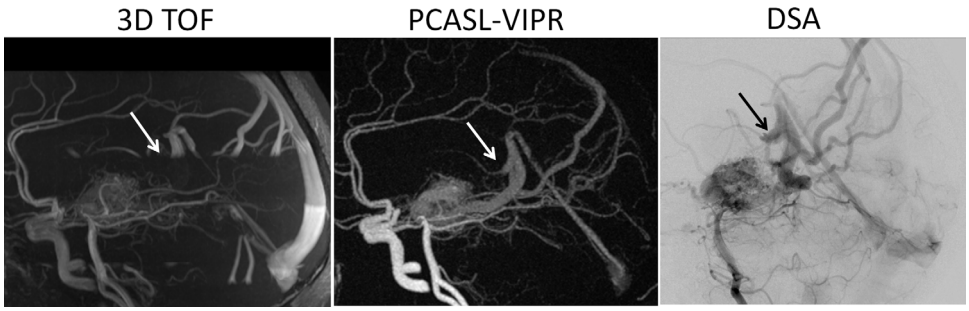

FIG. 3. Thalamic AVM patient: sagittal limited MIPs of 3D TOF (left), PCASL-VIPR (middle), and X-ray DSA (right). The arrows point to the venous drainage of the AVM into the vein of Galen. MIP image of 3D TOF shows severe signal loss in the draining vein due to saturation artifacts.

In the profile of PCASL-VIPR, signal is more uniform in the aneurysm and the signal drop due to slow flow is less compared to TOF. In this case, the labeling plane was unnecessarily lower (around the neck) than the other cases that caused longer transit time for the inverted spins to reach the disease. The signal drop due to T_1 recovery could also be observed in the basilar artery where the flow is slower than the internal carotid arteries. This kind of signal loss could be greatly reduced by proper adjustment of the labeling plane and higher signal in the aneurysm could have been obtained as well. Another reason that could result in signal loss is the reduced labeling efficiency due to off-resonance effects caused by field inhomogeneities at the labeling plane, but that has not been demonstrated in this case.

Table 2 summarizes the results from the qualitative evaluation. Pearson's correlation coefficient is 0.8, and the grading scores of two readers were averaged. For vessel visualization, PCASL-VIPR was superior in three of the eight vessel groups and pathology (positive values), whereas 3D TOF was slightly better in the other five vessel groups (negative values). However, there was no statistically significant difference between the two methods in any of these groups. For saturation artifacts, PCASL-VIPR was superior in four of the eight vessel groups and in the delineation of pathological conditions with a statistically significant advantage in visualization of the siphons (bold and underscored). 3D TOF was superior with no statistical significance in the remaining vessel comparisons. The scores were also averaged over all the evaluated vessel segments excluding pathology, and PCASL-VIPR performs slightly better in both criteria with no statistical significance.

Figure 7 shows the average CNR (mean ± SD) of PCASL-VIPR and 3D TOF across all subjects' vessel segment ROIs. Compared to 3D TOF, PCASL-VIPR shows higher CNR in the siphons and basilar artery (starred) with statistical significance (P value <0.05) and equal values in the others. The CNR values are also more consistent across the subjects in PCASL-VIPR. In addition, PCASL-VIPR shows a trend of signal diminishing from the siphons to the anterior cerebral arteries with increasing transit time.

DISCUSSION

We have developed a 3D noncontrast-enhanced MRA technique that combines ASL tagging with PCASL and an accelerated 3D radial acquisition technique, VIPR. PCASL-VIPR has been tested for intracranial angiography in both healthy and diseased subjects.

Compared with 3D TOF, PCASL-VIPR was found to hold several advantages over it as demonstrated by the images of the feasibility study. Ignoring the imperfect equalization of magnetization transfer (MT) effects and the tissue perfusion signal, static tissue should be completely cancelled out by subtraction procedure. With a near zero background, vessel visualization is limited by noise in the background rather than contrast with neighboring structures. PCASL has much less sensitivity to slow flow while 3D TOF suffers from saturation artifacts due to slow or in-plane flow patterns. When combined with a 3D radial trajectory, PCASL-VIPR can easily cover the entire head without the extension of scan time and achieve 3D isotropic spatial resolution simultaneously. According to our evaluation results, whole head PCASL-

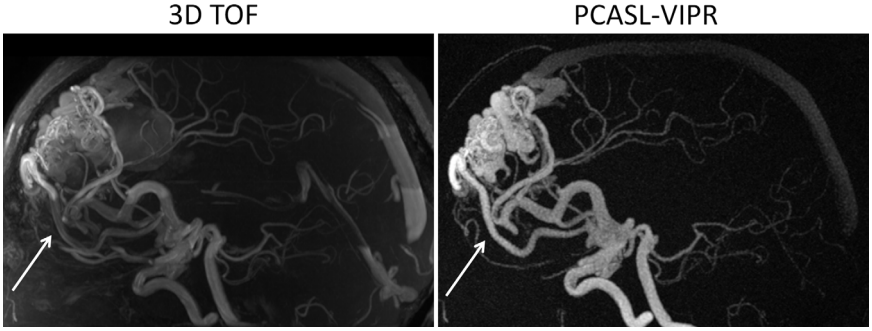

FIG. 4. Left frontal AVM patient: sagittal limited MIPs of 3D TOF (left) and PCASL-VIPR (right). The arrows point to the major feeding arteries of the AVM. Saturation artifacts can be observed in the feeding arteries in TOF image.

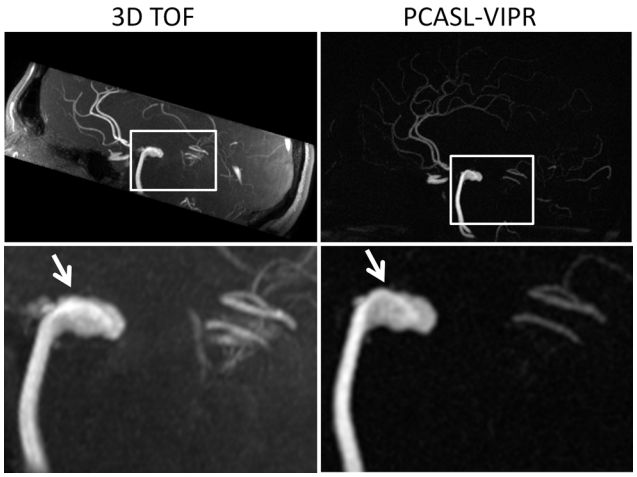

FIG. 5. Patient with an aneurysm at the tip of the basilar artery: sagittal limited MIPs (upper row) and the zoomed in view of the aneurysm (lower row) of 3D TOF (left) and PCASL-VIPR (right). Both exams show excellent visualization of the aneurysm. Little saturation artifact was seen in TOF image due to the fast flow in the aneurysm and small size. The bright region (arrows) depicts the inflow jet.

VIPR provides approximately equal image quality as 3D TOF in healthy subjects. When applied to patients especially, AVM patients, PCASL-VIPR provides better image quality and diagnostic information over 3D TOF that suffers from the artifacts due to saturation and multislab coverage. The recent large group study that investigated the reliability of using 3D TOF to follow up the obliteration process of AVMs (35) showed its insufficiency when the remaining nidus diameter is <10 mm. The reasons include spin dephasing due to complex or turbulent flow, saturation due to slow flow, and lack of temporal resolution. Our preliminary study has already shown PCASL's advantage of less sensitivity of slow flow. We also expect better performance of PCASL-VIPR in the delineation of AVMs when it is applied to dynamic angiography. In future study, systematic analysis of the AVM components with large number of subjects will be conducted.

PCASL-VIPR holds several advantages over previously developed 3D PASL angiography techniques (13,16,17). With PASL, the delay time between spin labeling and image acquisition needs to be chosen for the tradeoff between ensuring vasculature filling and providing adequate SNR. This parameter is subject dependent, and the selection requires additional scans and also induces other artifact issues, even with the retrospective methods. For this work, we were able to use a long label duration (3 s) that ensured adequate vessel filling. Longer label duration could be used but have diminished gains due to T_1 recovery of the tag. Second, the vessel segments with different transit times experience different amount of T_1 recovery in PCASL angiography varying from minimum (the proximal vessels) to maximum (the most distal vessels). In PASL angiography, all the vessel segments experience the same amount of T_1 recovery, which is determined by the longest transit time. Therefore, PCASL angiography provides higher SNR than PASL angiography.

Previously reported PCASL angiography (21,22) has demonstrated utility in acquiring hemodynamic vessel-specific information in intracranial angiography. However, these techniques are limited to 2D projection imaging or multiple thick-slab imaging, and cannot be easily extended to 3D imaging due to long scan times. With the accelerating benefits from the 3D radial trajectories, PCASL-VIPR is the first method to achieve high 3D isotropic spatial resolution that greatly improves the vessel visualization compared to the 2D techniques. PCASL-VIPR also holds the potential to depict temporal dynamics and label individual vascular beds. Temporal dynamics can be achieved by varying the label duration prior to imaging. Although dynamic contrast enhanced-MRA is also able to perform time-resolved imaging, temporal resolution and/or spatial resolution have to be compromised to match imaging data acquisition with the short

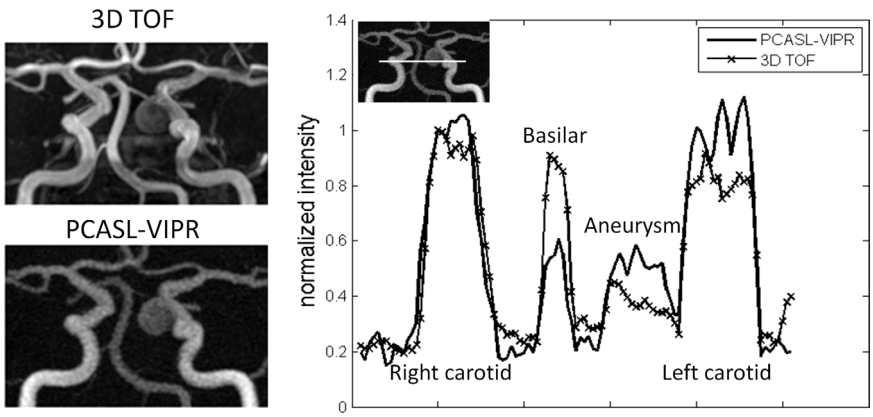

FIG. 6. Patient with an aneurysm arising from the left cavernous internal carotid artery: cropped coronal limited MIPs of 3D TOF (upper) and PCASL-VIPR (lower). PCASL-VIPR image shows stronger and more uniform signal inside the aneurysm and less blurring artifacts around it. The right figure shows the profile along the horizontal line across the aneurysm indicated in the left upper corner small image. Different vessels are labeled in the profile. 3D TOF profile (starred line) shows signal drop in the aneurysm and left carotid due to saturation of slow and recirculating flow. PCASL-VIPR shows weaker signal in the aneurysm and basilar artery due to the placing of the labeling plane.

Table 2
Results of Qualitative Evaluation

Evaluated vessel segments	Vessel visualization (1–4)			Saturation artifacts (1–4)		
	TOF	PCASL	PCASL-TOF[a]	TOF	PCASL	PCASL-TOF[a]
Anterior cerebral artery	3.25	3.10	−0.15	3.20	3.25	0.05
Right posterior cerebral artery	3.22	3.11	−0.11	3.22	3.06	−0.16
Left posterior cerebral artery	3.10	3.05	−0.05	3.15	3.05	−0.10
Right middle cerebral artery	3.35	3.30	−0.05	3.35	3.25	−0.10
Left middle cerebral artery	3.35	3.30	−0.05	3.35	3.25	−0.10
Basilar tip	3.40	3.45	0.05	3.35	3.50	0.15
Right siphon	3.30	3.60	0.30	3.30	3.85	**0.55**
Left siphon	3.25	3.60	0.35	3.30	3.85	**0.55**
Pathology	*2.80*	3.50	0.70	3.00	3.60	0.60
All the above vessels excluding pathology	3.28	3.32	0.04	3.28	3.39	0.11

[a]Score difference between PCASL-VIPR and 3D TOF. Positive values mean better performance of PCASL-VIPR over 3D TOF, negative values mean the opposite. Statistical significance as tested using a Wilcoxon signed rank test is indicated as underlined, and in bold font ($P < 0.05$). Values lower than 3 (not sufficient for diagnosis) are presented as Italic.

time period of the first pass of contrast agent. Additionally, the intravenous injection protocols lead to substantial bolus dispersion limiting the benefits of improved temporal resolution. For PCASL-based dynamic angiography, as the label duration is freely adjustable, inflow dynamics can be depicted with resolutions commonly achieved only with X-ray DSA. In practical use, the optimal temporal resolution is chosen to couple the sampling window that controls the amount of leading edge blurring due to the continuously advancing bolus and the diffuse artifacts caused by the inconsistency of the data. Although shortening the sampling window will proportionally increase the total scan time, the image with a short label duration will have greater sparsity and higher CNR to support higher acceleration factor when using VIPR acquisition. PCASL-VIPR is also capable of doing vessel-selective imaging based on PCASL's ability to target a specific feeding vessel, analogous to selective catheter injections in X-ray DSA. Time-resolved hemodynamic, and vessel-specific information similar to that obtained with DSA, without the use of exogenous contrast agents, makes PCASL-VIPR a promising alternative to X-ray DSA.

The efficacy of PCASL-VIPR is primarily limited by long scan times, T_1 recovery, RF-saturation, and labeling efficiency. Long scan times introduce sensitivity to motion artifacts and hinder time-resolved imaging. In this work, we have not used parallel imaging or compressed sensing (36) that could be used to help achieving higher acceleration factors. The signal difference of PCASL-VIPR is directly related to the labeling efficiency of PCASL. Efficiency can be degraded by imperfect phase tracking at the labeling plane. Phase tracking errors arise from off-resonance field at the labeling plane due to imperfect shimming or the susceptibility from eddy currents or gradient waveform errors. Corrections can be made if the amount of off resonance and gradient errors can be mapped at the labeling plane (37,38) but requires substantially more imaging time. Higher order shimming might also be useful and will be tested in future study.

Although signal saturation is substantially reduced compared to 3D TOF, signal loss is still observed in distal vessels in PCASL-VIPR. Because of T_1 recovery, signal decreases exponentially with the transit time from labeling plane. This limits the extent to which slow inflow can be imaged. In addition, signal saturation occurs in distal vessels due to the application of multiple RF pulses within an SPGR readout cycle. Spin that is not refreshed during the readout by inflow experiences more RF saturation. This effect is more severe when the readout flip angle increases and/or the acquisition window extends. The residual tissue signal at the inferior edge of the image volume as can be seen from the coronal and sagittal MIP images came from two sources: the selective inversion performed over the imaging volume and PCASL labeling at the edge of the volume. With PCASL, the tissue spins at the labeling plane experience (α, α) RF pulses in the label phase, and (α, $-\alpha$) RF pulses in the control phase. Therefore, the saturation effects caused by the two different RF pulse train are not equal. Furthermore, the selective inversion has a profile that will result in incomplete subtraction at areas just outside the imaging field of view. Subtraction of the label phase and control phase is not able to cancel out

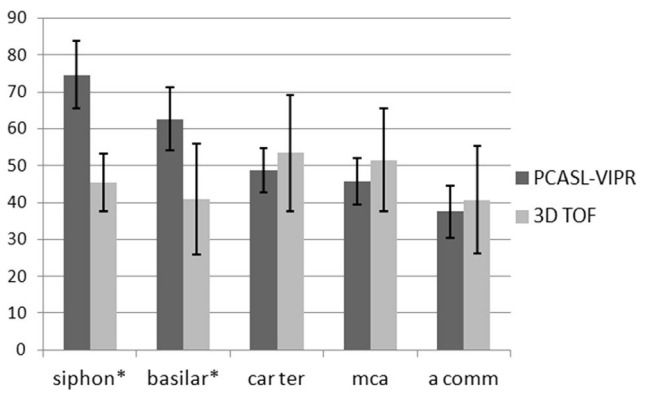

FIG. 7. CNR (mean ± SD) graph of PCASL-VIPR and 3D TOF measured from five ROIs: left/right siphons, basilar tip, left/right carotid terminus (car ter), first bifurcation spot of the middle cerebral arteries (mca), and 5-mm region around the anterior communicating artery (a comm). CNR of PCASL-VIPR is higher than 3D TOF in siphons and basilar tip (starred) with statistical significance tested by *t* test. It also shows signal decreases in moving from proximal to distal vessels. CNR of 3D TOF shows no flow related decay pattern; the standard deviation is higher (less consistent across the subjects).

the tissue signal at the labeling plane and leaves some residual tissue signal at the inferior edges of the 3D image volume. Both of these errors would be mitigated by placing the labeling plane more inferior, at the cost of reduced flow sensitivity.

The use of bSSFP as seen in other noncontrast enhanced-MRA methods could provide higher SNR and reduced RF saturation effects. However, SSFP is generally more prone to off-resonance artifacts that are more prevalent when imaging at higher field strength. In this work, the choice of SPGR avoided this issue and also reduced the specific absorption rate compared to bSSFP. All acquisitions in this study were obtained at 3 T, which provides higher SNR over 1.5 T and decreased T_1 recovery thanks to longer T_1.

In conclusion, a novel noncontrast-enhanced 3D MRA technique is presented in this study. The feasibility of this technique was validated for intracranial angiography. Other potentials such as time-resolved imaging and vessel selective imaging will be developed in future work. PCASL-VIPR will be further validated by being applied to larger patient groups and compared to conventional X-ray DSA.

ACKNOWLEDGMENTS

We acknowledge GE Healthcare for their assistance and support. The authors thank Yijing Wu for helpful discussions.

REFERENCES

1. Xu J, Kochanek K, Murphy S, Tejada-Vera B. Deaths: final data for 2007. Natl Vital Stat Rep 2007;58(19).
2. Grohn O, Kauppinen R. Assessment of brain tissue viability in acute ischemic stroke by BOLD MRI. NMR Biomed 2001;14:432–440.
3. Grandin CB. Assessment of brain perfusion with MRI: methodology and application to acute stroke. Neuroradiology 2003;45:755–766.
4. Atlas SW, Thulborn KR. Intracranial hemorrhage. In: Atlas SW, ed. Magnetic resonance imaging of the brain and spine, 3rd ed. Philadelphia: Lippincott Williams & Wilkins; 2002. pp 773–832.
5. Parker DL, Yuan C, Blatter DD. MR angiography by multiple thin slab 3D acquisition. Magn Reson Med 1991;17:434–451.
6. Axel L. Blood flow effects in magnetic resonance imaging. AJR Am J Roentgenol. 1984;143:1157–1166.
7. Haider C, Borisch E, Glockner J, Mostardi P, Rossman P, Young P, Riederer S. Max CAPR: high-resolution 3D contrast-enhanced MR angiography with acquisition times under 5 seconds. Magn Reson Med 2010;64:1171–1181.
8. Velikina JV, Johnson KM, Wu Y, Samsonov AA, Turski P, Mistretta CA. PC HYPR flow: a technique for rapid imaging of contrast dynamics. J Magn Reson Imaging 2010;31:447–456.
9. Wu Y, Kim N, Korosec FR, Turk A, Rowley HA, Wieben O, Mistretta CA, Turski PA. 3D time-resolved contrast-enhanced cerebrovascular MR angiography with subsecond frame update times using radial k-space trajectories and highly constrained projection reconstruction. AJNR Am J Neuroradiol 2007;28:2001–2004.
10. Miyazaki M, Lee VS. Nonenhanced MR angiography. Radiology 2008;248:20–43.
11. Miyazaki M, Akahane M. Non-contrast enhanced MR angiography: established techniques. J Magn Reson Imaging 2012;35:1–19.
12. Nishimura DG, Macovski A, Pauly JM, Conolly SM. MR angiography by selective inversion recovery. Magn Reson Med 1987;4:193–202.
13. Tan ET, Huston J 3rd, Campeau NG, Riederer SJ. Fast inversion recovery magnetic resonance angiography of the intracranial arteries. Magn Reson Med 2010;63:1648–1658.
14. Johnson KM, Wieben O, Block WF, Mistretta CA. Accelerated time resolved inflow imaging with 3D radial bSSFP. In ISMRM Workshop on Data Sampling and Image Reconstruction, Sedona, Arizona, USA, 2009.
15. Chen Q, Mai VM, Storey P, Edelman RR. Dynamic ASL flow imaging with cardiac triggered true FISP acquisition. In Proceedings of the 9th Annual Meeting of ISMRM, Glasgow, Scotland, 2001. p. 1956.
16. Yan L, Wang S, Zhuo Y, Wolf RL, Stiefel MF, An J, Ye Y, Zhang Q, Melhem E, Wang DJJ. Unenhanced dynamic MR angiography: high spatial and temporal resolution by using true FISP-based spin tagging with alternating radiofrequency. Radiology 2010;256:270–279.
17. Bi X, Weale P, Schmitt P, Zuehlsdorff S, Jerecic R. Non-contrast-enhanced four-dimensional (4D) intracranial MR angiography: a feasibility study. Magn Reson Med 2010;63:835–841.
18. Dai W, Garcia D, de Bazelaire C, Alsop D. Continuous flow-driven inversion for arterial spin labeling using pulsed radio frequency and gradient fields. Magn Reson Med 2008;60:1488–1497.
19. Wong E. Vessel-encoded arterial spin-labeling using pseudocontinuous tagging. Magn Reson Med 2007;58:1086–1091.
20. Koktzoglou I, Gupta N, Edelman R. Nonenhanced extracranial carotid MR angiography using arterial spin labeling: improved performance with pseudocontinuous tagging. J Magn Reson Imaging 2011;34:384–394.
21. Robson P, Dai W, Shankaranarayanan A, Rofsky N, Alsop D. Time-resolved vessel-selective digital subtraction MR angiography of the cerebral vasculature with arterial spin labeling. Radiology 2010;257:507–515.
22. Okell TW, Chappell MA, Woolrich MW, Gunther M, Feinberg DA, Jezzard P. Vessel-encoded dynamic magnetic resonance angiography using arterial spin labeling. Magn Reson Med 2010;64:698–706.
23. Barger AV, Block WF, Toropov Y, Grist TM, Mistretta CA. Time-resolved contrast-enhanced imaging with isotropic resolution and broad coverage using an undersampled 3D projection trajectory. Magn Reson Med 2002;48:297–305.
24. Hargreaves BA, Cunningham CH, Nishimura DG, Conolly SM. Variable-rate selective excitation for rapid MRI sequences. Magn Reson Med 2004;52:590–597.
25. Kim SG. Quantification of relative cerebral blood flow change by flow-sensitive alternating inversion recovery (FAIR) technique: application to functional mapping. Magn Reson Med 1995;34:293–301.
26. Bieri O, Scheffler K. Flow compensation in balanced SSFP sequences. Magn Reson Med 2005;54:901–907.
27. Peters DC, Korosec FR, Grist TM, Block WF, Holden JE, Vigen KK, Mistretta CA. Undersampled projection reconstruction applied to MR angiography. Magn Reson Med 2000;43:91–101.
28. Holmes BH, O'Halloran RL, Brodsky EK, Jung Y, Block WF, Fain SB. 3D hyperpolarized He-3 MRI of ventilation using a multi-echo projection acquisition. Magn Reson Med 2008;59:1062–1071.
29. Altbach MI, Outwater EK, Trouard TP, Krupinski EA, Theilmann RJ, Stopeck AT, Kono M, Gmitro AF. Radial fast spin-echo method for T2-weighted imaging and T2 mapping of the liver. J Magn Reson Imaging 2002;16:179–189.
30. Theilmann RJ, Gmitro AF, Altbach MI, Trouard TP. View-ordering in radial fast spin-echo imaging. Magn Reson Med 2004;51:768–774.
31. Beatty PJ, Nishimura DG, Pauly JM. Rapid gridding reconstruction with a minimal oversampling ratio. IEEE Trans Med Imaging 2005;24:799–808.
32. McKenzie CA, Yeh EN, Ohliger MA, Price MD, Sodickson DK. Self-calibrating parallel imaging with automatic coil sensitivity extraction. Magn Reson Med 2002;47:529–538.
33. Griswold MA, Jakob PM, Nittka M, Goldfarb JW, Haase A. Partially parallel imaging with localized sensitivities (PILS). Magn Reson Med 2000;44:602–609.
34. Roemer PB, Edelstein WA, Hayes CE, Souza SP, Mueller OM. The NMR phased array. Magn Reson Med 1990;16:192–225.
35. Buis DR, Bot JC, Barkhof F, Knol DL, Lagerwaard FJ, Slotman BJ, Vandertop WP, van den Berg R. The predictive value of 3D time-of-flight MR angiography in assessment of brain arteriovenous malformation obliteration after radiosurgery. AJNR Am J Neuroradiol 2012;33:232–238.
36. Lustig M, Donoho D, Pauly JM. Sparse MRI: the application of compressed sensing for rapid MR imaging. Magn Reson Med 2007;58:1182–1195.
37. Jung Y, Wong EC, Liu T. Multiphase pseudocontinuous arterial spin labeling (MP-PCASL) for robust quantification of cerebral blood flow. Magn Reson Med 2010;64:799–810.
38. Jahanian H, Noll D, Hernandez-Garcia L. B(0) field inhomogeneity considerations in pseudo-continuous arterial spin labeling (pCASL): effects on tagging efficiency and correction strategy. NMR Biomed 2011;24:1202–1209.